THE EUROPEAN
PHYSICAL JOURNAL D

Excited-state dynamics of deuterated indigo

Trevor Cohen[1], Nathan Svadlenak[1], Charles Smith[1], Krystal Vo[1], Si-Young Lee[1], Ana Parejo-Vidal[1], Joseph R. A. Kincaid[1], Andrzej L. Sobolewski[2], Michal F. Rode[2], and Mattanjah S. de Vries[1,a]

[1] Department of Chemistry and Biochemistry, University of California Santa Barbara, Santa Barbara, CA 93106-9510, USA
[2] Institute of Physics, Polish Academy of Sciences, al. Lotnikow 32/46, 02-668 Warsaw, Poland

Abstract. Indigo, a rich blue dye, is an incredibly photostable molecule that has survived in ancient art for centuries. It is also unique in that it can undergo both an excited-state hydrogen and proton transfer on the picosecond timescale followed by a ground-state back transfer. Previously, we performed gas phase excited-state lifetime studies on indigo to study these processes in a solvent-free environment, combined with excited-state calculations. We found two decay pathways, a fast sub-nanosecond decay and a slow decay on the order of 10 ns. Calculations of the excited-state potential energy surface found that both hydrogen and proton transfer are nearly isoenergetic separated by a 0.1 eV barrier. To further elucidate these dynamics, we now report a study with deuterated indigo, using resonance-enhanced multi-photon ionization and pump-probe spectroscopy with mass spectrometric isotopomer selection. From new calculations of the excited-state potential energy surface, we find sequential double-proton or hydrogen transfer, whereby the trajectory to the second transfer passes a second barrier and then encounters a conical intersection that leads back to the ground state. We find that deuteration only increases the excited-state lifetimes of the fast decay channel, suggesting tunneling through the first barrier, while the slower channel is not affected and may involve a different intermediate state.

1 Introduction

Since antiquity, dyes obtained from animal parts, bugs, and plants have been used to produce vibrant colors for painting on a variety of art media. One such dye, indigo, has been used in many ancient civilizations such as the Roman and Maya empires and was highly sought after for its brilliant deep blue color [1, 2]. Indigo can be observed throughout history due to its stability, especially against photodamage, rendering it still visible on many pieces of art [3]. This inherent stability also explains the popularity of this dye to this day. High photostability is directly correlated with a fast excited-state relaxation mechanism which can be modeled through excited-state dynamics studies.

Upon absorption of light, a molecule must be able to return to the ground state at a fast rate to prevent other damaging reactions from occurring. Such fast internal conversion often proceeds via conical intersections [4]. In the case of indigo, the excited molecule initially undergoes an excited-state intramolecular hydrogen or proton transfer (ESIHT or ESIPT) tautomerizing from the diketo to the keto–enol conformer. Yamazaki et al.

followed by Moreno et al. were the first to calculate this relaxation mechanism through excited-state calculations mapping part of the energy surface [5, 6]. Berenbeim et al. [7] showed that blocking the path to excited-state intramolecular proton transfer through hydroxyl substitution in anthraquinone dyes greatly increased the excited-state lifetimes. The excited-state lifetimes of various forms of indigo such as indigo carmine and leuco-indigo were measured in solution and were found to depend on solvent polarity [8–13].

Previously, we studied the excited-state dynamics of indigo in the gas phase using resonance-enhanced two-photon ionization (R2PI) in combination with excited-state calculations [14]. Pump-probe spectroscopy performed in both the picosecond and nanosecond time regimes revealed two distinct decay channels. While the calculated potential energy surfaces reveal that indigo can undergo ESIPT or ESIHT, both processes are generally known to be sub-picosecond events and would therefore be too fast to directly measure with our laser systems. We therefore proposed that the two measured lifetimes reflect dynamics of the keto–enol tautomer that forms from these transfers, with the faster decay tentatively assigned to that of the tautomer formed from ESIPT and the slower from ESIHT. Excitation to a vibronic state below 800 cm^{-1} resulted in lifetimes on the order of a nanosecond for the faster channel and 10–20 ns for the slower channel. Upon excitation
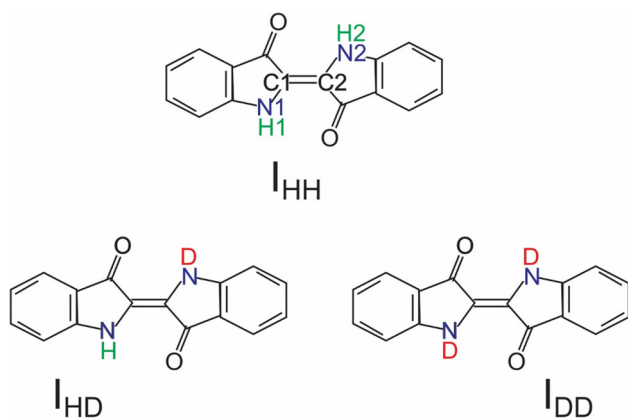
Fig. 1 The chemical structures of I_{HH}, I_{HD}, and I_{DD}. All three forms of indigo are assumed to be only observable in the trans-diketo tautomer in the cold jet before excitation

at higher excess energy, we only observed a single fast decay that decreased in lifetime with increasing energy to 105 ps at 1456 cm^{-1} and down to 60 ps at 1859 cm^{-1}.

Deuteration has been used extensively in excited-state dynamics studies involving proton and hydrogen transfers to measure kinetic effects by increasing the mass of the transferring atom. Green et al. [15] found deuteration of Criegee intermediates slowed the rate of formation of hydroxyl radicals, indicating a proton transfer was involved. Bodi et al. [16] found that the deuteration of acetone ions slowed the PT tunneling process 100-fold completely shutting off the pathway to form methane. In solution, studies of deuterated indigo carmine revealed a longer excited-state lifetime, suggesting that the proton most likely tunneled through the barrier [17, 18]. Excited-state calculations found that the barrier to proton transfer in indigo is dependent on the distance between the N and O atoms, revealing the amino hydrogens in the diketo form are the target site for the ESIPT and ESIHT [19, 20].

In this study, we deuterated the two sites on indigo capable of proton or hydrogen transfer to measure and analyze the effect on the excited-state dynamics (see Fig. 1). Additionally, we present further calculations of the potential energy surface of indigo, revealing that transfer of a second-proton or hydrogen leads to a conical intersection region and back to the ground state. Using mass selective R2PI experiments, we independently measured the dynamics of indigo (I_{HH}), monodeuterated indigo (I_{HD}), and di-deuterated indigo (I_{DD}). We found that only the fast process showed a kinetic isotope effect, pointing to a different mechanism than previously proposed for the slow decay. I_{HD} measurements revealed that the order of hydrogen or deuteron transfer has a major effect on the measured excited-state lifetimes, suggesting the transfer mechanism is sequential, consistent with the shape of the excited-state potential energy surface.

2 Methods

2.1 Computational

The equilibrium geometry of the most stable form of the indigo molecule in its closed-shell ground electronic state (S_0), the planar diketo form (Fig. 1A), was determined with the MP2 method [21] with C_s symmetry constraint. The minimum energy of the S_0 state is the reference value for all other ground-state and excited-state structures. The excited-state (S_1) equilibrium geometries were determined with the second-order algebraic diagrammatic construction ADC(2) method [22–25]. The correlation-consistent valence double-zeta basis set with polarization functions on all atoms (cc-pVDZ) [26] was used in these calculations as well as in the calculations of potential energy profiles and surfaces.

To study the reaction paths of the two active protons in the excited state of the diketo form, relaxed potential energy profiles were calculated; first, along the first NH coordinate, R_1 (N1-H), and subsequently along the second NH coordinate, R_2 (N2-H). For each fixed value of a given NH coordinate the remaining internal nuclear coordinates were optimized.

To reveal the mechanism of the double-proton transfer process, relaxed potential energy surfaces were calculated in the ground state and in the excited state. The two NH stretching coordinates R_1 and R_2 were fixed, while the remaining nuclear coordinates were optimized for a given state. All calculations were performed using the TURBOMOLE program package [27].

2.2 Experimental

The deuterated indigo was synthesized in a two-step, one-pot process (Fig. 2). Indigo was purchased from Sigma-Aldrich (95% purity). Because indigo has very low solubility with most solvents in its base structure, it was reduced to leuco-indigo and dissolved in a bath of NaOH, sodium dithionate, and then deuterated at the target sites. After 3 h of heating at 80 °C, oxygen bubbled through the solution and the deuterated indigo was precipitated out. This resulting product consisted of a mixture of I_{HH}, I_{HD}, and I_{DD}. Each indigo was identified and present in the product and confirmed through monitoring in a time-of-flight mass spectrometer.

We have described R2PI spectroscopy and pump-probe experiments in detail previously and will briefly summarize them here [28]. The deuterated indigo was placed on a graphite bar and loaded into the chamber ($\sim 2 \times 10^{-6}$ torr). A 1064-nm laser (Continuum Minilite I, 5-ns pulse width) is focused onto the graphite bar, desorbing and vaporizing the sample with minimal fragmentation. To continuously refresh the desorption area with new material, the sample stage is translated orthogonal to the desorption laser. To jet-cool the sample gas, a molecular beam of argon is pulsed into the chamber (8 atm backing pressure, 30 μs pulse width),
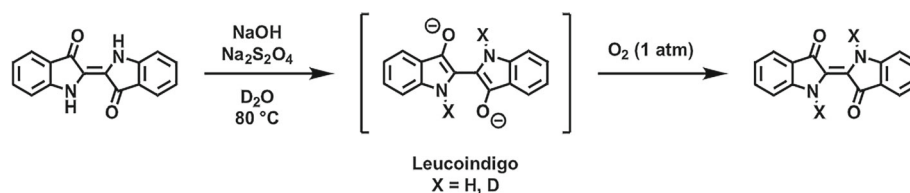
Fig. 2 The reaction scheme for the synthesis of deuterated indigo. Indigo sample is reduced to its leuco-form, heated, and undergoes deuterium exchange with deuterated water. The solution is then oxidized resulting in a mixture of I_{HH}, I_{HD}, and I_{DD}

entraining the sample in a supersonic jet. Through collisions with the argon, the sample is cooled to ˜ 15 K and directed into the sub-chamber of the mass spectrometer through a skimmer.

Both resonant two-photon ionization (R2PI) and pump-probe spectroscopy were used for characterization and analysis of the excited-state dynamics in the ns and ps time regime. For the R2PI experiments on the ps timescale, the third harmonic of an EKSPLA PL2251 Nd:YAG laser (30 ps pulse width, 1064 nm fundamental) pumped an EKSPLA PG-401 tunable optical parametric generator (OPG). This system produces 6.5 cm^{-1} linewidth, 30 ps, ˜ 600-μJ pulses in the visible wavelength region. The OPG is scanned from 500 to 560 nm to resonantly excite the molecule to the S1 state. For ionization, the fundamental and second harmonic produced from the pump laser is combined to generate the 5th harmonic (213 nm). To measure excited-state lifetimes, the ionization laser is mechanically delayed with a Thorlabs 300 mm mechanical delay stage with a retroreflector providing a delay of up to approximately 2000 ps. For measurements with longer delay times, the scannable pulse generated from the ps OPG system was coupled with a 213-nm pulse generated from a Quantel DCR-11 Nd:YAG laser (5 ns, 8 mJ/pulse). The picosecond OPG pulse and ns DCR-11 pulse were delayed electronically with a Stanford Instruments DG-645 delay generator to measure ns pump probes. For both ns and ps pump-probe experiments, the relative ion count is measured as a function of the delay of the ionization laser and convolved and fitted to either a monoexponential or biexponential decay in a Mathematica script [29]. The signal to noise in the data and the pulse width of the lasers limit the precision with which we can derive lifetimes from this fitting procedure. For the pump-probe spectra obtained with ps ionization pulses the precision is 100 ps; for the pump-probe spectra obtained with ns ionization pulses the precision is 3 ns.

3 Results

3.1 Experimental results

Figure 3 shows the R2PI spectra for I_{HH}, I_{HD}, and I_{DD}, obtained with 213-nm, 30-ps ionization pulses. Excitation wavelength is given as excess energy beyond
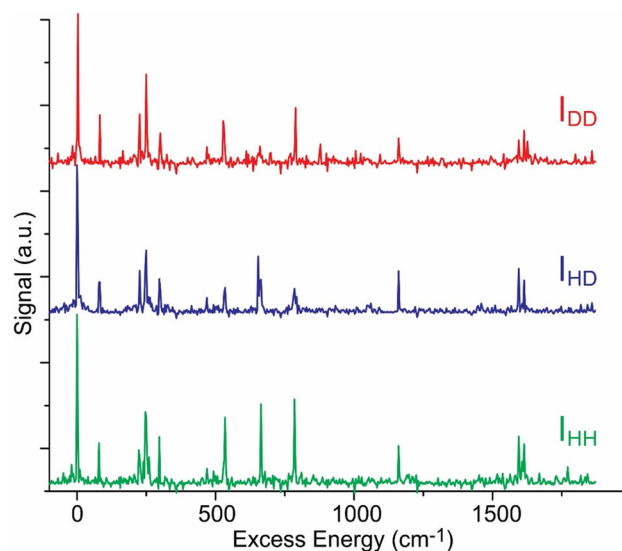

Fig. 3 R2PI spectra for I_{HH} (green), I_{HD} (purple), and I_{DD} (red), obtained with 30 ps excitation pulse and 213 nm, 30-ps ionization pulse without delay

the origin, which for I_{HH} is at 18,129 cm^{-1}. I_{DD} blue shifts approximately 6–10 cm^{-1} relative to I_{HH}. We observed vibronic lines up till about 1800 cm^{-1} excess energy, with decreasing excited-state lifetimes beyond about 1000 cm^{-1} (vide infra). For I_{HH} we previously found from IR-UV double-resonant spectroscopy that the diketo tautomer of indigo was the only species observed in our experiment [14]. We assume the same holds true for I_{HD} and I_{DD}. Thus, we assigned all the vibronic transitions in each of the isotopomers to this tautomer. The I_{DD} excitation peaks shift approximately 6–10 cm^{-1} to the blue of the corresponding I_{HH} peaks, depending on the vibrational mode. The I_{HD} peaks are broader than those for I_{HH} and I_{DD} and include the excitation wavelengths of both isotopomers. We interpret this observation as absorption by either the undeuterated or the deuterated chromophore. Therefore, the excitation wavelength selects whether the excited-state dynamics is initiated by the proton or the deuterium transfer, as further discussed below. The line width of the ps laser system (6.5 cm^{-1}) is too broad to fully resolve each peak corresponding to the hydrogen or deuterium chromophore excitation resulting in the broadened feature.

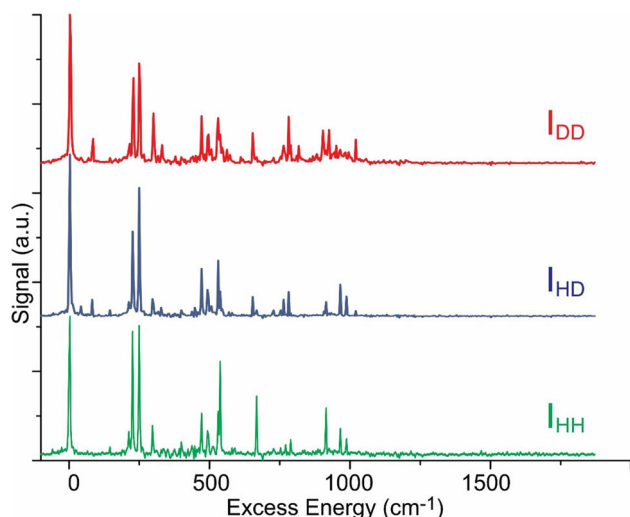Figure 4 shows the R2PI spectra obtained with

Fig. 4 R2PI spectra for (green) I_{HH}, (purple) I_{HD}, and (red) I_{DD}, obtained with 30-ps excitation pulse and 213-nm, 6-ns ionization pulse without delay

ns ionization (213-nm, 6-ns pulses). A nanosecond pulse width ionization laser cannot efficiently ionize excited states with lifetimes below 1 ns. In our previous work, with ns ionization we did not observe transitions beyond 725 cm^{-1} excess energy, suggesting the existence of a barrier beyond which the excited-state lifetime is too short for ns ionization. The current work revealed transitions up to 987 cm^{-1} excess in energy. In I_{HD} and I_{DD} we measured transitions up to 1020 cm^{-1} in excess energy.

We measured the excited-state lifetimes of I_{HH}, I_{HD}, and I_{DD} in the picosecond and nanosecond regimes at each vibronic transition in the R2PI spectrum using pump-probe spectroscopy. Figures 5 and 6 show sample picosecond and nanosecond pump-probe spectra and exponential fitting at the origin transition. Additional ps and ns pump-probe spectra examining the PES of I_{HD} and I_{DD} can be found in Figs. S1–4. Table 1 lists the excited-state lifetimes of I_{HH} and I_{DD} in the ps and ns regime as well as the corresponding ratios of those lifetimes, which represent the kinetic isotope effect (KIE). For the slow decay we do not observe a KIE, with the value equal to 1 within the margin of error. Like I_{HH}, I_{DD} exhibits two lifetimes: A fast decay observed with ps ionization, which we denote as τ_{1H} and τ_{1D} and a slow decay observed with ns ionization, denoted as τ_{2H} and τ_{2D}. The average kinetic isotope effect below the barrier was 4 for the faster decay, while we observed no effect for the slower process. Beyond the 1000 cm^{-1} excess energy transition, we did not observe the slow decay corresponding to τ_{2H} and τ_{2D}, while for the fast decay both τ_{1H} and τ_{1D} decrease with increasing energy.

In monodeuterated indigo, I_{HD}, it may make a difference whether the deuterated or the undeuterated chromophore is excited. Since the excitation of I_{DD} is blue-shifted by 6 cm^{-1}, we assume that in the case of I_{HD} the deuterated chromophore absorbs at 6 cm^{-1} to the blue

of the undeuterated chromophore. The two excitations were not fully resolvable since the linewidth of the laser was too broad, and therefore at each given wavelength a mixture of the deuterated and non-deuterated chromophores was excited, resulting in a convolution of the two excited-state lifetimes which we analyzed as follows. For each vibronic I_{HD} peak below the barrier, we measured two pump-probe spectra, one at the I_{HH} wavelength and one at the I_{DD} wavelength. We assumed that each decay trace corresponded to a combination of decays from each chromophore, whereby the contribution from the H-chromophore and D-chromophore is larger at the I_{HH} and I_{DD} wavelength, respectively. Thus, using the lifetimes and the peak wavelength obtained for I_{HH} and I_{DD}, we calculated the contribution of each chromophore excitation at a given transition. Table 2 lists these contributions for the ps and ns timescale, respectively.

The presence of C-13 isotopes complicates the interpretation of these spectra. The signal from the I_{HH} mass spectrum is entirely due to I_{HH}; however, the I_{HD} mass peak is formed by a combination of I_{HD} molecules and I_{HH} molecules with a C-13 isotope. For example, denoting molecules with a C-13 isotope with a prime, the signal at I + 1 M/Z is the result of $(I_{HD} + I'_{HH})$. The signal at the $I + 2$ M/Z is the result of $(I_{DD} + I'_{HD})$. With a 1.1% natural C-13 abundance, 16.2% of all indigo molecules have at least one C-13 atom. The occurrence of multiple C-13 isotopes on a single molecule is below our noise threshold.

We derived the relative abundances of the deuterated chromophores by solving for all six species present in our mass signals: I_{HH}, I'_{HH}, I_{HD}, I'_{HD}, I_{DD}, I'_{DD} (I'_{DD} does not become convoluted with our other signals because it occurs at mass $I + 3$), using the following equations:

$$I = I_{HH}$$
$$I + 1 = I_{DH} + I'_{HH}$$
$$I + 2 = I_{DD} + I'_{HD}$$
$$(0.162)I_{HH} - (0.838)I'_{HH} = 0$$
$$(0.162)I_{HD} - (0.838)I'_{HD} = 0$$
$$(0.162)I_{DD} - (0.838)I'_{DD} = 0$$

Solving for these variables allowed us to determine the relative abundances of the various deuterated species. This correction was only needed for the I_{HD} signal, which was split between the $I + 1$ and $I + 2$ M/Z mass peaks.

3.2 Computational results

Figure 7 shows two minimum energy potential-energy (PE) profiles of the S_0 (dashed lines) and S_1 (solid lines) states of indigo calculated at the ADC(2)/cc-pVDZ level along minimum-energy paths optimized in the S_1 state. The NH coordinate was frozen in these
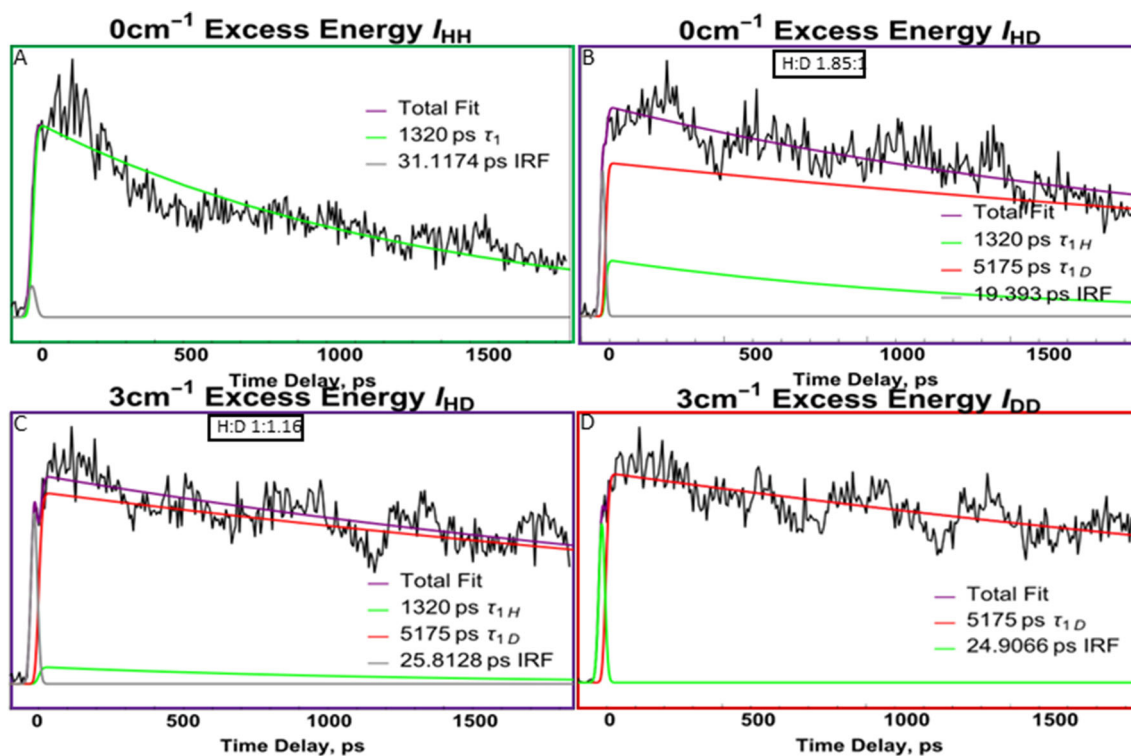
Fig. 5 Picosecond pump-probe spectra for **A** I_{HH}, **B** and **C** I_{HD}, **D** I_{DD}. The experimental data in the case of I_{HH} are those of reference 7. For each fit of the exponential decays, the faster hydrogen transfer decay is in green, the slower deuterium transfer in red, and the total fit in purple. The instrument response function (IRF) is gray

Fig. 6 Nanosecond pump-probe spectra for **A** I_{HH}, **B** and **C** I_{HD}, **D** I_{DD}. For each fit of the exponential decays, the hydrogen transfer decay is in green, the deuterium transfer in red, and the total fit in purple. The instrument response function (IRF) is gray

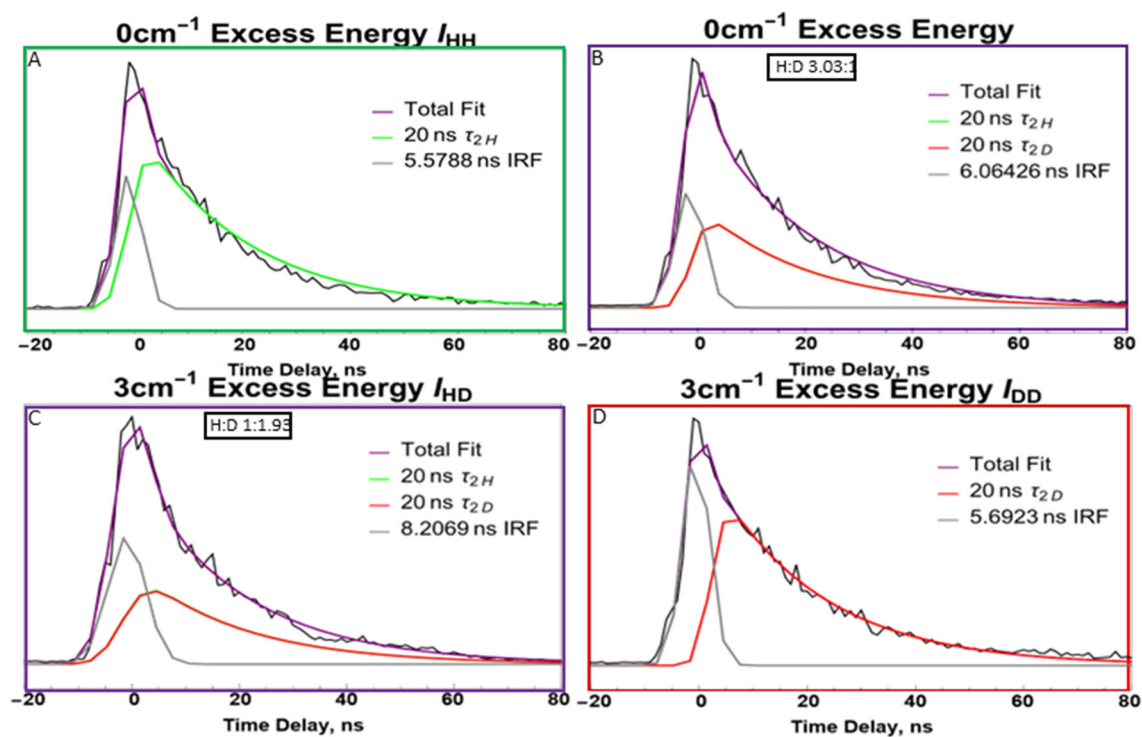**Table 1** Excited-state lifetimes for I_{HH} and I_{DD} at various relative energies above the origin transition as well as the calculated kinetic isotope effect (KIE)

Excess energy above I_{HH} origin (cm^{-1})	τ_{1H} (ps)	τ_{1D} (ps)	KIE τ_1	τ_{2H} (ns)	τ_{2D} (ns)	KIE τ_2	Excess energy above I_{DD} origin (cm^{-1})
0	1320	5172	3.9	20.0	20.0	1.0	3
79	887	4999	5.6	22.4	20.6	0.9	83
297	1353	2209	1.6	9.2	15	1.6	300
531	2017	5779	2.9	13.3	16	1.2	527
654		2092			14		
664	1540			8.6			
785	692	1955	2.8	8.6	8.4	0.95	789
1161	168	638	3.8				
1595		321					
1614	79	314	4.0				

The excess energies with corresponding I_{DD} vibronic transitions are in parentheticals. The lifetimes of the fast decay for I_{HH} and I_{DD} are denoted τ_{1H} and τ_{1D} and τ_{2H} and τ_{2D} for the slow decay

Table 2 Observed picosecond lifetimes for I_{HD}

Excess energy (cm^{-1}) (chromophore excited labeled with H or D)	Wavelength (nm)	τ_1 (ps)	τ_{1H}:τ_{1D}	τ_2 (ns)	τ_{2H}:τ_{2D}
0(H)	551.6		1.0:2.7		3.0:1
3(D)	551.5		1.0:11		1:1.9
79(H)	549.2		2.0:1		1:60
83(D)	549.1		1.2:1		28:1
297(H)	542.7		1.0:7.7		8200:1
300(D)	542.6		2.8:1		2.0:1
527(H)	536		1:4.5	13	
664(D)	532.4	973			
667(H)	532.3	717		10	
785(D)	528.7		2.8:1		100:1
789(H)	528.6		4600:1		500:1
1161(H)	518.4	170			
1595(H)	507	77			
1614(H)	506.5	89			

Since the respective H and D chromophores were not fully resolvable, the lifetimes in the fitted decays were fitted to the I_{HH} and I_{DD} lifetimes and the ratio of the normalized pre-exponential factors is reported. For peaks that were fully resolvable and showed monoexponential decay, the excited-state lifetimes were reported in the τ_1 column

calculations, while the rest of the parameters were optimized in the S_1 state. We obtained two PE profiles, which we denote as X (red) and Y (blue). The PE profiles of the X and Y conformers are represented by red triangles and blue squares, respectively. The left panel plots the PE profile along the R_1 coordinate, representing an initial excited-state proton transfer for X and hydrogen transfer for Y. This profile has a barrier, B1, of approximately 0.1 eV. The right panel plots the PE profile along the second N–H coordinate, R_2, representing a subsequent second H/H$^+$ transfer. After the first transfer, indigo enters a local minimum forming the keto–enol tautomer, from which the second transfer can proceed toward the enol–enol tautomer.

The Cartesian coordinates of the S1(X) and S1(Y) structures are given in SI. The S1(X) and S1(Y) structures are two different excited-state conformers distinguished with different optimized geometry (in the S_1 state) and electronic structure obtained as two different solutions of the ADC(2)/cc-pVDZ method. They differ, for example, in dipole moments and the C_1–C_2 distances (see Fig. S6). The X and profiles are nearly
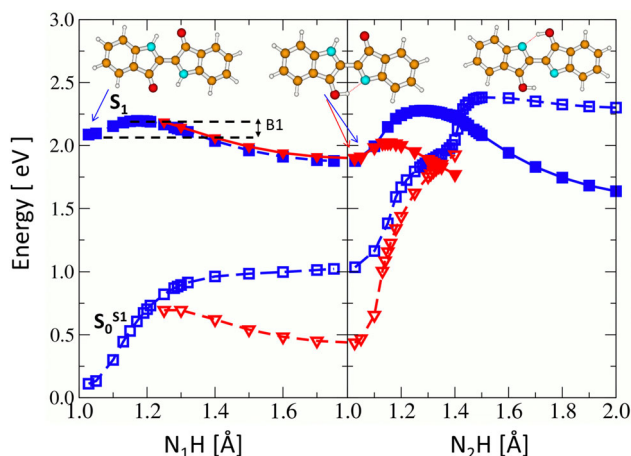
Fig. 7 Two minimum energy profiles of indigo (calculated at the ADC(2)/cc-pVDZ level) plotted as a function of N_1-H distance (left panel, first ESIPT) and N_2-H distance (right panel, second ESIPT). Solid lines denote minimum-energy profiles of the S_1 state. Dashed lines (S_0^{S1}) denote energy profiles of the S_0 state computed at the optimized geometries of the S_1 state. See text for details

degenerate in the Frank–Condon region with a barrier between them of less than 0.01 eV [14]. However, these profiles deviate in energy along the second H/H$^+$ transfer coordinate. We identify X as the result of proton transfer and Y as the result of hydrogen transfer upon excitation. X and Y are further distinguished by a different C_1–C_2 distance for the keto–enol form, which is 1.454 Å for X and 1.382 Å for Y. This difference between X and Y is maintained along the entire range of both N1-H and N2-H stretching coordinates. The S_1-state proton transfer profile, X, is characterized also by geometries with a larger S_1-state dipole moment, μ_e, than for the S_1-state hydrogen transfer, Y. In the enol–keto form μ_e equals 6.8D for X and 3.4D for Y. Along the path of second the H/H$^+$ transfer we found a barrier (B2) of 0.124 eV for X at N2H = 1.14 Å and significantly higher barrier of 0.401 eV for Y at N2H = 1.28 Å. Beyond that barrier we found a conical intersection along both X and Y reaction paths that leads back to the ground state followed by ground-state intramolecular proton or hydrogen transfer back to the diketo form.

Figure 8 shows relaxed potential-energy surfaces of (A) the electronic ground state and (B) the lowest excited state of the Y form, plotted as a function of the two stretching coordinates R_1(N1-H) and R_2(N2-H). As the molecule is symmetric with respect to exchange of these two coordinates, the plots keep the same symmetry as well. As can be seen in panel A, the diketo form is the lowest energy tautomer in the S_0 ground state, and it is the dominant population in our experiment. In both S_0 and S_1 there is a very large barrier for a concerted double-proton or hydrogen transfer to form the dienol tautomer which would be represented by a diagonal movement up and to the right in Fig. 8. The barrier calculated along this path is significantly higher in

energy than the barrier for the sequential double transfer, and this process therefore is not probable. Thus, the shape of the PE surfaces indicates the possible mechanism of sequential two proton/hydrogen transfer processes, both in the S_0 and S_1 electronic states as exothermic pathways. Figure S3 in supplemental information shows the IR-vibrational modes, that involve N–O or O–H motion, calculated with the TD-DFT/B3-LYP/cc-pVDZ method, for the S_1, diketo form.

4 Discussion

We previously calculated intramolecular proton or hydrogen transfer pathways along a single NH coordinate, essentially covering only the left-hand panel in Fig. 7. That work did not elucidate a clear mechanism down to the ground state. We hypothesized that keto–enol indigo could undergo a non-radiative process back to the ground-state potential and that decay in the Y form would be faster based on a smaller energy gap between the excited and ground states compared to X. In this work we extended the computations to include a second-proton transfer, represented in the right-hand panel of Fig. 7. We conclude that the X and Y trajectories differ along that second coordinate and that there is a conical intersection with the ground state along that part of the trajectory behind a barrier, B2. For the Y form, the conical intersection is at higher energy and B2 is higher than for the X form. Experimentally, we measured excited-state lifetimes for deuterated indigo and observed a KIE for the faster decay and not for the slower decay. A complete modeling of these new observations will require future dynamics calculations, but absent those we can speculate about some possible explanations.

Based on our original double-resonant spectroscopy, only the diketo tautomer is observed in our experiment, implying that both measured decays must derive from excitation of this same species. If the two lifetimes would originate from decay of the same initial excited state, the significantly slower 20-ns decay would have an order of magnitude smaller quantum yield and would not be observed in this experiment, since most signal would derive from the faster mechanism. We therefore propose that, following excitation to the keto–keto excited state, a bifurcation takes place in which one trajectory follows the X part of the S1 surface with proton transfer, exhibiting a larger dipole moment, μ_e, and stretching of the C_1–C_2 bond, and the other trajectory follows the Y part with hydrogen transfer, a smaller μ_e, and a shorter C_1–C_2 distance. Each trajectory leads to a different form of keto–enol indigo, each with different excited-state lifetimes.

It is possible for the X trajectory to proceed through the conical intersection as indicated by the red curves in Fig. 7. Our earlier work indicated that the ground-state X PE surface involves a hydrogen (rather than proton) transfer, which implies that the transition from
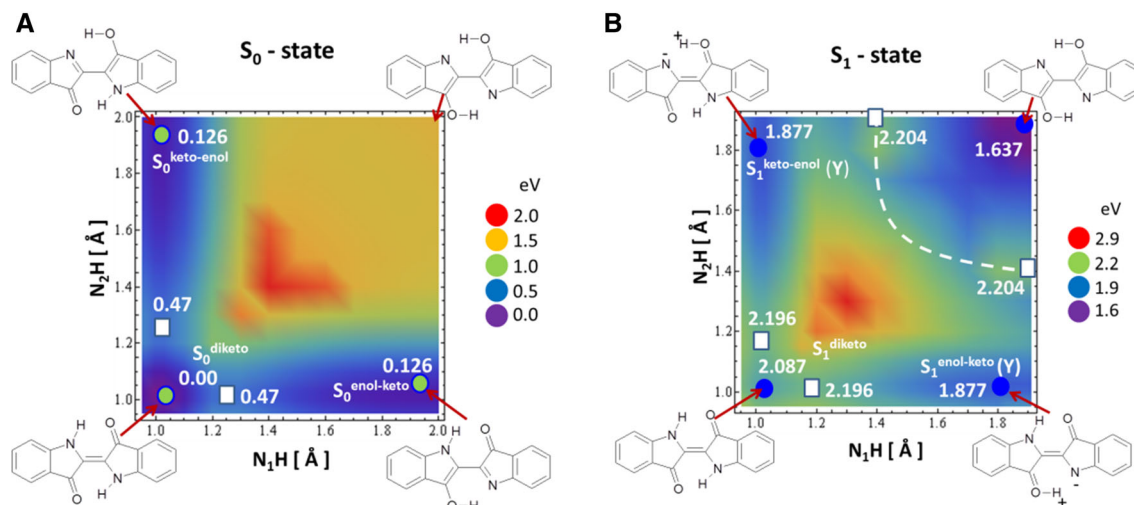
Fig. 8 Relaxed potential-energy surfaces of (**A**) the electronic ground state and (**B**) the lowest excited state of the indigo molecule, plotted as a function of the two stretching coordinates R_1 and R_2. Green circles represent ground-state diketo (global) and single-proton transferred enol–keto (local) minima. Blue circles represent S_1^{diketo}, $S_1^{\text{enol-keto}}$, and S_1^{dienol} minima. The dashed white line shows the S_1/S_0 conical intersection seam. The results were obtained with the ADC(2)/cc-pVDZ method for the excited state and with the MP2/cc-pVDZ method for the ground state. Relative energies of minima and barriers are given in eV

S_1 to S_0 along this path involves an electron transfer. If we assume that the first-proton transfer is subpicosecond, then with our lifetime measurements we are merely observing the dynamics of the resulting KE tautomer that is formed, with X decaying faster than Y. However, if we assume that the observed KIE is due to passing (or tunneling through) the first barrier, then the shorter lifetimes reflect the dynamics of the first part of the X trajectory, which is dominated by the first-proton transfer but not at sub-picosecond rates.

Assigning the slower decay to the Y form, we note that the initial part of the trajectory is almost identical to that of the X form, but with hydrogen rather than proton transfer. We would still expect a similar KIE effect for that first part of the trajectory, but if the decay of the subsequent keto–enol form does not exhibit a KIE, we would not observe the initial small change of lifetime in our ns timescale measurements. There are a number of possible models for the slower decay of the keto–enol Y form.

(1) We rule out tunneling through the large, 0.4-eV second barrier, B2, to reach the conical intersection on the Y profile because we observe no KIE on the long lifetime decay. (2) When the system is trapped in the excited-state keto–enol minimum, it may interconvert by non-adiabatically populating the X form, from which it can decay to the ground state. (3) Another pathway from the long-lived Y keto–enol excited state could be fluorescence. From the energy and oscillator strength computed at the optimized geometries of the S1 state (CC2/cc-pVDZ optimization of the S1 state), we estimate a radiative lifetime of 11.2 ns. This qualitatively reflects our observation. We note that for the keto–keto form, the calculated radiative lifetime is 5.5 ns, so while we cannot rule out fluorescence for this form, it is an unlikely explanation given the observed KIE. (4) These

scenarios do not explain the fact that the slow channel cannot be observed in the ns regime above about 0.1 eV excess energy. Therefore, we should also consider the possibility of exploring other parts of the PE landscape along other internuclear coordinates that might lead to population of other long-lived states, such as an $n\pi^*$ state or a triplet state.

I_{HD} provides a unique system since it breaks the symmetry of the molecule. Deuteration of only one of the chromophores acts as a spectroscopic tag that reveals which of the two chromophores is excited at a given transition. Even though the bandwidth of our ps laser system is limited, excitation at the I_{HH} peak wavelength will preferentially excite the hydrogen containing chromophore (Φ_{H}), while excitation at the I_{DD} peak wavelength will preferentially excite the deuterated chromophore (Φ_{D}). When Φ_{H} is excited, H (or H$^+$) will transfer first; when Φ_{D} is excited, D (or D$^+$) will transfer first. Analysis of the I_{HD} decays in the picosecond regime shows that when exciting Φ_{D}, the decay is slower than when exciting Φ_{H}, consistent with the model in which the decay rates are dominated by the first transfer, rather than the second. This result is consistent with the calculations that predict a concerted double-proton or hydrogen transfer is not occurring, as in that case the rate would not change between each chromophore excitation unlike other similar double-proton transfer mechanisms [30].

5 Conclusions

We have reported the R2PI spectra for I_{HD} and I_{DD} as well as their excited-state lifetimes at each measured vibronic transition. There are two decay channels, a

faster and a slower one. Deuterating both chromophores results in a KIE of ˜ 4 for the faster channel but has no effect on the slower channel. Directly comparing the excited-state lifetimes of each chromophore independently in I_{HD} reveals that exciting the deuterated chromophore increases the excited-state lifetime. Calculations of the excited-state potential energy surfaces show trajectories with sequential double-proton or hydrogen transfer. Along the path to the second transfer a conical intersection occurs to the ground state with a barrier approximately 0.1 eV high. Two potential-energy profiles are involved, X and Y with different C_1–C_2 distances and characterized by excited-state proton transfer for X and hydrogen transfer for Y. The barrier to the conical intersection for Y is significantly higher than for X, most likely indicating that for the fast decay excited indigo relaxes to the ground state along the X potential. The longer lifetime channel likely reflects the decay from the keto–enol form along the Y potential energy profile. Further insights will be expected from excited-state dynamics computations to model of these results.

Author contributions

TC performed experiments and analysis and wrote manuscript, NS contributed to experiments, analysis, and manuscript, CS, KV, SYL, and APV performed experiments, JK conceived of and performed synthesis, AS and MR developed theoretical model, MR performed computations, MdV provided experimental setup, performed analysis, and edited final version of manuscript.

Data availability statement This manuscript has no associated data, or the data will not be deposited. [Authors' comment: Data consist of raw experimental spectra, which will not ne deposited.].

References

1. R.J.H. Clark, C.J. Cooksey, M.A.M. Daniels, R. Withnall, Endeavour **17**(4), 191 (1993)
2. J.C. Splitstoser, T.D. Dillehay, J. Wouters, A. Claro, Sci. Adv. **2**(9), e1501623 (2016)
3. R.M. Christie, Biotech. Histochem. **82**(2), 51 (2007)
4. J.A. Otterstedt, J. Chem. Phys. **58**(12), 5716 (1973)
5. S. Yamazaki, A.L. Sobolewski, W. Domcke, Phys. Chem. Chem. Phys. **13**(4), 1618 (2011)
6. M. Moreno, J.M. Ortiz-Sanchez, R. Gelabert, J.M. Lluch, Phys. Chem. Chem. Phys. **15**(46), 20236 (2013)
7. J. Berenbeim, S. Boldissar, S. Owens, M.R. Haggmark, C. Gatto, F.M. Siouri, T. Cohen, M.F. Rode, C. Schmidt-Patterson, M.S. de Vries, Sci. Adv. **5**, eaaw5227 (2019)
8. J. Pina, D. Sarmento, M. Accoto, P.L. Gentili, L. Vaccaro, A. Galvao, J.S.S. de Melo, J. Phys. Chem. B **121**(10), 2308 (2017)
9. N.D. Bernardino, S. Brown-Xu, T.L. Gustafson, D.L.A. de Faria, J. Phys. Chem. C **120**(38), 21905 (2016)
10. I. Iwakura, A. Yabushita, T. Kobayashi, Chem. Lett. **38**(11), 1020 (2009)
11. J.S. de Melo, A.P. Moura, M.J. Melo, J. Phys. Chem. A **108**(34), 6975 (2004)
12. P.P. Roy, J. Shee, E.A. Arsenault, Y. Yoneda, K. Feuling, M. Head-Gordon, G.R. Fleming, J. Phys. Chem. Lett. **11**(10), 4156 (2020)
13. Y. Nagasawa, R. Taguri, H. Matsuda, M. Murakami, M. Ohama, T. Okada, H. Miyasaka, Phys. Chem. Chem. Phys. **6**(23), 5370 (2004)
14. M.R. Haggmark, G. Gate, S. Boldissar, J. Berenbeim, A.L. Sobolewski, M.S. de Vries, Chem. Phys. **515**, 535 (2018)
15. A.M. Green, V.P. Barber, Y. Fang, S.J. Klippenstein, M.I. Lester, Proc. Natl. Acad. Sci. U. S. A. **114**(47), 12372 (2017)
16. A. Bodi, T. Baer, N.K. Wells, D. Fakhoury, D. Klecyngier, J.P. Kercher, Phys. Chem. Chem. Phys. **17**(43), 28505 (2015)
17. A.S. Chatterley, D.A. Horke, J.R.R. Verlet, Phys. Chem. Chem. Phys. **14**(46), 16155 (2012)
18. I. Iwakura, A. Yabushita, T. Kobayashi, Chem. Phys. Lett. **484**(4–6), 354 (2010)
19. A. Douhal, F. Lahmani, A.H. Zewail, Chem. Phys. **207**(2–3), 477 (1996)
20. J.A. Syage, J. Phys. Chem. **99**(16), 5772 (1995)
21. C. Moller, M.S. Plesset, Phys. Rev. **46**, 618 (1934)
22. C. Hattig, Adv. Quantum Chem. **50**(50), 37 (2005)
23. J. Schirmer, Phys. Rev. A **26**(5), 2395 (1982)
24. A.B. Trofimov, J. Schirmer, J. Phys. B At. Mol. Opt. **28**(12), 2299 (1995)
25. D. Tuna, D. Lefrancois, L. Wolanski, S. Gozem, I. Schapiro, T. Andruniow, A. Dreuw, M. Olivucci, J. Chem. Theory Comput. **11**(12), 5758 (2015)
26. T.H. Dunning, J. Chem. Phys. **90**(2), 1007 (1989)
27. TURBOMOLE (2016).
28. G. Meijer, M.S. Devries, H.E. Hunziker, H.R. Wendt, Appl. Phys. B Photo **51**(6), 395 (1990)
29. F.M. Siouri, S. Boldissar, J.A. Berenbeim, M.S. de Vries, J. Phys. Chem. A **121**(28), 5257 (2017)
30. K. Sakota, H. Sekiya, J. Phys. Chem. A **109**(12), 2722 (2005)